Dynamic Telemetry Link Advantage When Tracking a Lunar Orbiter with a 34-m Antenna at 2.3 GHz and 8.4 GHz

David D. Morabito*

ABSTRACT. — The amount of data that can be sent on telemetry links for tracking spacecraft depends upon the signal-to-noise power ratio. Both spacecraft and ground system can be sized to determine and optimize the amount of received signal power. The noise power depends on a variety of contributors, but for most NASA deep-space interplanetary missions, the receiver noise temperature is usually ~20 K or higher depending upon elevation angle. Given that near-Earth missions such as those to the Moon depend more and more on larger-diameter antennas such as those of the NASA Deep Space Network (DSN), the added hotbody noise of the lunar disk can be significant, resulting in overall system noise temperatures of ~200 K or higher. This significant increase can severely affect data rates and its variation as a ground antenna tracks a lunar orbiter needs to be characterized.

I. Introduction

The Moon reflects visible sunlight and thus will take on distinct appearances during its 29.5-day synodic cycle as viewed from Earth. The amount of lunar infrared emission is well correlated with the lunar phase cycle, originating from a very thin surface layer. However, at radio and microwave wavelengths, the amount of this variation is less as the emission originates within deeper surface layers. At microwave wavelengths, the emission is dominated by thermal noise that is related to the Moon's surface and near-surface temperature, which in turn is related to the properties of the lunar surface material and received solar insolation.

The amount of data that can be sent on telemetry links for tracking spacecraft depends upon the signal-to-noise power ratio. Both spacecraft and ground system can be sized to determine and optimize the amount of received signal power. The noise power depends on a variety of contributors, but for most NASA deep-space interplanetary missions, the receiver

* Communications Architectures and Research Section.

The research described in this publication was carried out by the Jet Propulsion Laboratory, California Institute of Technology, under a contract with the National Aeronautics and Space Administration.

noise temperature is usually ~20 K or higher, depending upon elevation angle and frequency band. Given that near-Earth missions such as those to the Moon depend more and more on larger-diameter antennas such as those of the NASA Deep Space Network (DSN), the added hotbody contribution of the lunar disk can be significant, resulting in overall system noise temperatures of ~200 K or higher. The amount of increase depends upon antenna diameter, observing frequency, lunar phase angle, and location on the lunar disk where the ground antenna beam is centered. This significant increase can severely affect data rates, and its variation as a ground antenna tracks a lunar orbiter needs to be understood in order to assess optimal data return strategies.

A previous study [1] reported on the first comprehensive analysis of observing an extended source using a large-diameter DSN antenna at microwave frequencies. This study included a physical optics characterization of the noise temperature increase as a function of lunar phase for a 34-m-diameter antenna pointed at the center of the Moon. These "predictions" were then compared against direct measurements at three DSN frequency bands: 2.3 GHz (S-band) where the antenna beamwidth is comparable to the lunar diameter, and 8.4 GHz (X-band) and 32 GHz (Ka-band) where the beamwidth is a small fraction of the lunar diameter. It was found that the physical-optics-predicted noise temperatures were in agreement with the measured noise temperatures at the few-percent level.

Several robotic missions are now being flown and many more missions are being considered to revisit the Moon, both human and robotic. Such missions will employ very high data rates and thus will require accurate estimates of all contributions in telecommunications link calculations, including lunar thermal noise contributions. This additional system noise temperature increase using a large-diameter antenna tracking a lunar orbiter is further complicated by the changing contributions as the orbiter traverses the lunar disk. These include the variation of brightness over the lunar disk and changing contributions of disk and cold sky within the ground antenna beam.

A nominal telecommunications link budget usually assumes the worst-case noise temperature in order to set a single data rate to be used over the entire orbit. By dynamically changing the data rate to accommodate changing conditions, such as elevation angle, and thermal hotbody noise pickup, a larger data volume could be realized during an orbit. This study provides a first-order examination of this increased link advantage, which we can define as the data volume achieved by changing the data rate divided by the data volume achieved using a single "worst-case" static data rate. We will examine how this advantage varies for different lunar orbit scenarios at 2.3 GHz and 8.4 GHz. A future study will characterize this advantage for near-Earth 26-GHz telemetry links using a 34-m-diameter antenna.

II. Observations and Calibrations

The Research and Development (R&D) DSN 34-m-diameter antenna DSS-13 was used to acquire a series of measurements of noise temperature while pointed at the center of the lunar disk as well as tracking Lunar Reconnaissance Orbiter (LRO) in its orbit around the Moon. The total power radiometer (TPR) at DSS-13 [2] was used to simultaneously record the 2.3-GHz and 8.4-GHz system noise temperature measurements on dual channels. The

use of a dichroic mirror allowed for the simultaneous 2.3-GHz and 8.4-GHz observations. These measurements were used to evaluate link advantage as a function of orbiter location on the disk of the Moon relative to disk-centered pointing. The disk-centered measurements served as "worst-case" reference points. Since the amount of lunar noise changes significantly during an orbit, these measurements can allow for examination of dynamic link scenarios (changing data rate as the system-to-noise ratio changes) to increase overall data volume.

The measured system noise temperature includes contributions from the antenna, receiver equipment, Earth's atmosphere, and lunar hotbody noise. Depending on link frequency, antenna diameter, and antenna boresight position on the lunar disk, the lunar noise contribution will depend on an integration of the antenna beam with the lunar disk and any cold sky that falls into the beam. The cold-sky background noise temperature is expected to be equal to the cosmic microwave background (~2.7 K) and the lunar disk temperature will depend on the brightness distribution of the Moon picked up by the ground antenna beam, which is also a function of lunar phase angle and link frequency. The 2.3-GHz beam for a 34-m-diameter antenna on Earth is comparable to the lunar disk angular extent. The 8.4-GHz beam size is significantly smaller than the extent of the lunar disk.

The nominal sequence of events conducted during a lunar noise temperature pass can be seen graphically for the case of 2014-045 (February 14, 2014) at 2.3 GHz and 8.4 GHz, as seen in Figures 1 and 2, respectively. These events include (a) a series of calibrations at zenith to allow accurate conversion of system noise temperature from power meter readings at both 2.3 GHz and 8.4 GHz, (b) a sequence of noise temperature measurements pointing the antenna beam at the center of the lunar disk, at the limbs of the lunar disk in both cross-elevation directions (parallel to the horizon), and at cold sky (at +3 deg and –3 deg in cross-elevation, or parallel to the horizon). This was followed by tracking LRO as it orbited both in front of and behind the Moon in order to establish a reasonable noise temperature signature. The LRO noise temperature measurements were then followed by another series of disk-centered and cold-sky noise temperature measurements of shorter duration. The calibrations at the start of each pass made use of ambient loads and noise diodes in addition to cold-sky measurements performed at zenith [2].

Spectrum analyzer measurements of LRO's 2.3-GHz carrier peak and adjacent noise floor were also taken to allow for measurement of carrier power to noise density (P_cN_0) for comparison against predicted P_cN_0 values such as provided in [3]. Bandpass filters were inserted at the power meter input of the TPR to ensure that no signal energy from LRO's 2.3-GHz signal would contaminate the noise temperature measurements. There is no emission at 8.4 GHz from the spacecraft.

The overall noise temperature signatures for pass 2014-045 at 2.3 GHz and 8.4 GHz are depicted in Figures 1 and 2, respectively. The alphabetic annotations (A) through (F) on Figures 1 and 2 can be correlated with the locations of LRO in its orbit around the Moon at these same instances, as depicted in images generated by the Satellite Orbit Analysis Program (SOAP) [4] (see Figure 3). For instance, note the difference in the measured noise temperature for points (B) and (F) in Figures 1 and 2 when LRO is at an altitude of 179 km (see Figure 3) from the lunar surface as compared to point (D) showing a higher noise tem-

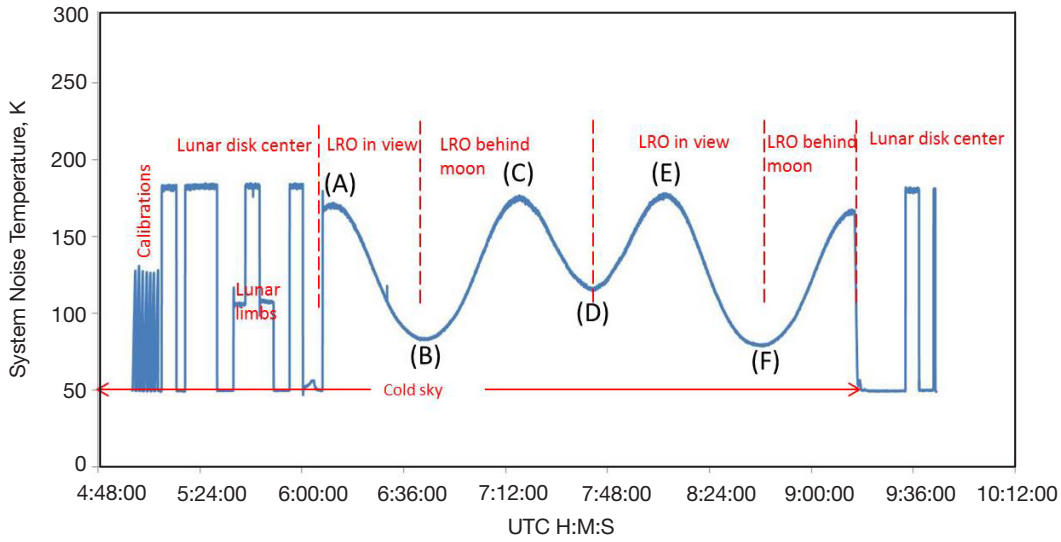

Figure 1. 2.3-GHz noise temperature measurements during DSS-13 tracking pass 2014-045 with annotations.

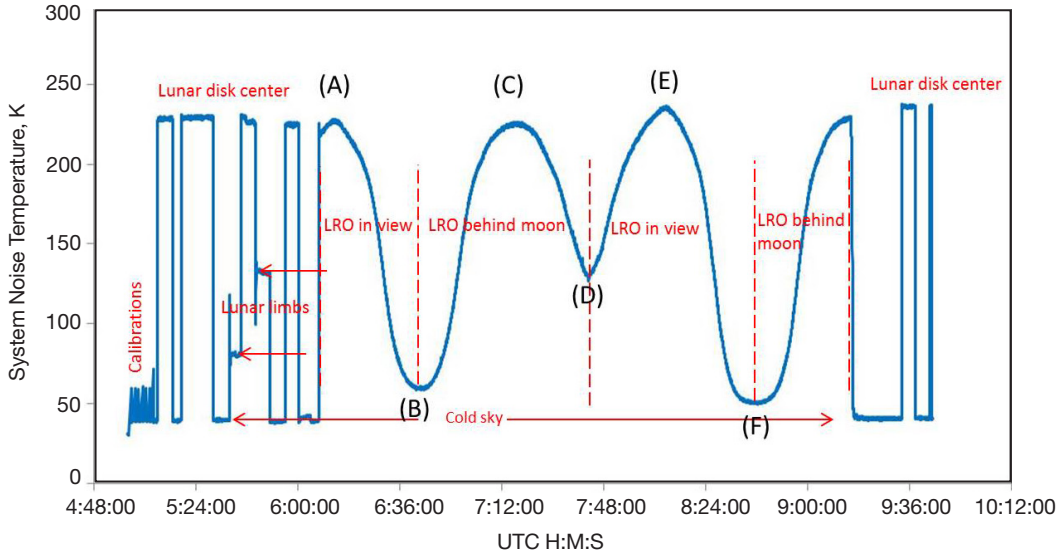

Figure 2. 8.4-GHz noise temperature measurements during DSS-13 tracking pass 2014-045 with annotations.

perature when its altitude is 36 km above the lunar surface in the plane of the sky. When LRO is at the higher altitude above the lunar surface (in the plane of the sky), the ground antenna beam picks up more of the lower noise temperature cold sky and less of the higher noise temperature of the lunar disk, resulting in a lower net noise temperature. When the ground antenna beam is pointed at LRO while it is above and close to the disk center, a significantly higher lunar noise temperature contribution is obtained and much less of the cold sky. This results in a much higher noise temperature contribution, as seen at points A and E in Figures 1 and 2. Point (C) depicts the sub-point scenario when the ground antenna beam is close to the disk center while tracking LRO (which is behind the Moon). The effect of the lunar phase angle (illumination fraction) is not shown in the SOAP plots presented in this article.

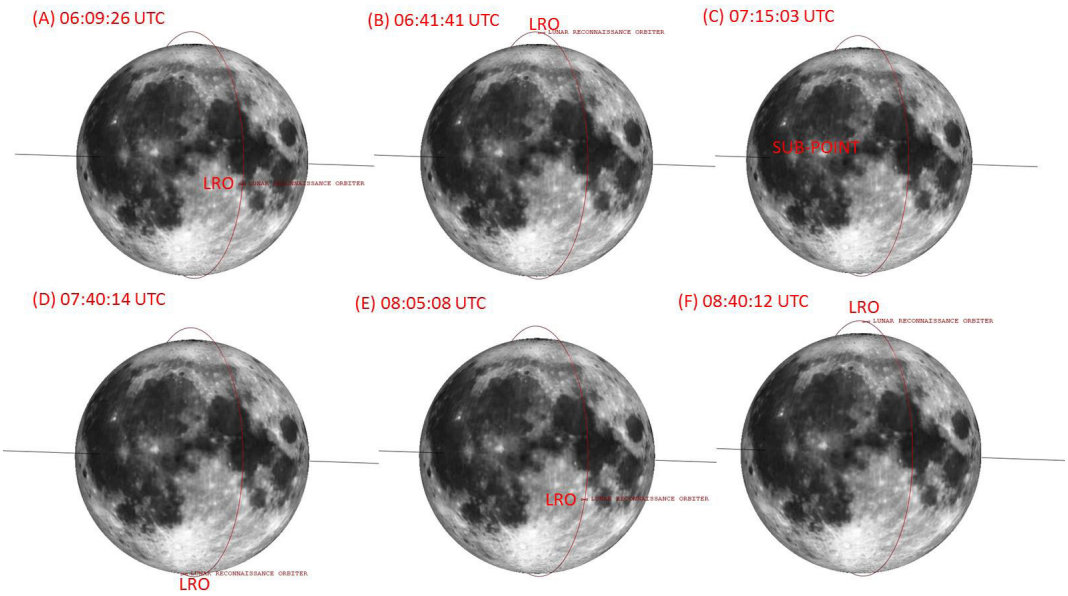

Figure 3. SOAP images of the Moon on 2014-045 showing location of LRO in its orbit during selected times. Lunar phase angle = 179 deg (full moon). The red "LRO" icon shows LRO's location at the indicated UTC time for each case.

Table 1 displays a summary of the estimated disk-centered lunar noise temperature measurements for each of the passes conducted at the S-/X-band feed position at DSS-13, along with the lunar phase angle and the average elevation angle over the pass. T_{Moon} is the measured noise temperature increase relative to background level (cold sky removed) when the antenna beam is pointed at the center of the lunar disk. The corrected T_{Moon} includes an atmospheric correction for the provided mean elevation angle to allow for a comparison against the earlier measurement set or predictions [1] for validation purposes. The predictions from [1] served as a computational model in order to check the integrity of the ambient load calibrations performed at zenith. From earlier studies, it was believed the computational model has an accuracy of ~3 percent. It was found that at S-band the disk-centered lunar noise temperature measurements were in agreement with the computational model within its quoted accuracy. However, it was found that a scale factor of 0.95 was required at X-band to yield agreement between the disk-centered lunar noise temperature measurements and the computational model. The need for this scale factor was attributed to uncertainties in the low-noise amplifier and follow-on temperature values used in the X-band calibrations. The statistics of the resulting disk-centered measurements were found to be in reasonable agreement with those from the previous campaign [1]. Figure 4 displays the physical-optics-derived model from [1] (solid curves) along with the corrected T_{Moon} measurements (single data points) from Table 1. The calibrations produced results that are accurate to the ~4 percent level, both systematic and random. At 2.3 GHz, there is little variation with lunar phase, whereas some variation can be inferred at 8.4 GHz upon examination of Figure 4. The effect of the ~4 percent calibration error on the link advantage results will be discussed later.

Passes conducted on 2013-189, 2013-274, 2013-275, 2013-276, and 2013-312 were calibration test passes at the S-/X-band feed position and did not involve the tracking of LRO.

Table 1. Summary of estimated disk-centered lunar noise temperature measurements.

Pass	Day of Year	Days Past Jan 1, 2013	Lunar Phase Angle, deg	Elevation Angle, deg	T_{Moon} (S), K	Corrected T_{Moon} (S), K	T_{Moon} (X), K	Corrected T_{Moon} (X), K
2013-189	189	189	0.7	14.5	128.5	133.2	176.0	182.4
2013-274	274	274	339.1	54.1	135.1	136.6	185.5	187.6
2013-275	275	275	349.6	44.6	135.3	137.0	181.3	183.6
2013-276	276	276	356.6	34.5	135.5	137.7	180.6	183.5
2013-312	312	312	65.2	14.5	132.5	137.3	173.6	180.0
2014-037	37	402	95.1	56.9	127.6	129.0	182.9	184.9
2014-045	45	410	178.9	54.4	133.2	134.7	187.5	189.6
2014-047	47	412	183.5	49.5	130.7	132.2	198.3	200.6
2014-049	49	414	199.9	41.3	130.4	132.2	194.5	197.1
2014-051	51	416	228.9	34.8	131.5	133.5	184.9	187.8
2014-055	55	420	326.5	28.4	131.4	133.9	192.3	196.0
2014-058	58	423	353.2	36.3	134.9	136.9	192.0	195.0
2014-065	65	430	63.3	59.4	130.1	131.5	178.5	180.4
2014-070	70	435	133.0	59.5	127.7	129.1	185.0	187.0
2014-073	73	438	169.5	54.1	128.2	129.6	192.2	194.3
2014-076	76	441	180.9	42.3	132.0	133.8	195.5	198.1

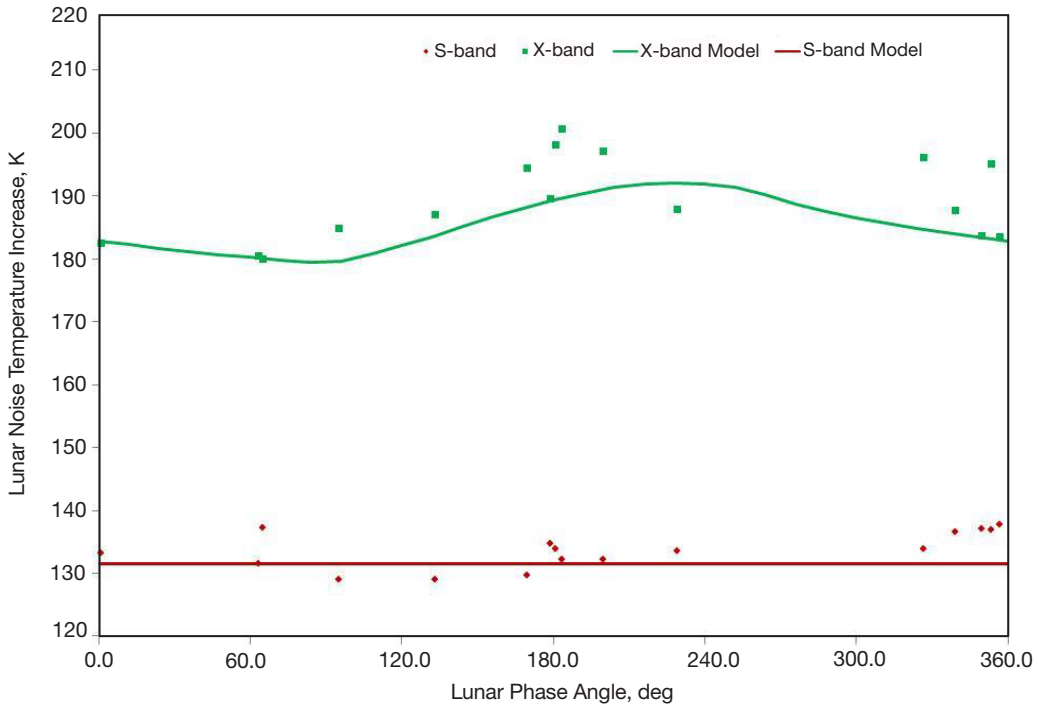

Figure 4. Lunar noise temperature increase versus lunar phase angle for models for 2.3 GHz (red curve) and 8.4 GHz (green curve) and corrected measurements for 2.3 GHz (red points) and 8.4 GHz (green points). Full moon occurs at 180 deg; new moon occurs at 0 deg.

Other passes conducted in 2013 included lunar disk temperature measurements in addition to raster scans and drift scans of the Moon. Pass 2013-276 was the first pass where LRO was tracked; however, there were issues with additional noise at 8.4 GHz. Another pass conducted on 2013-312 produced useful data, but lacked detailed calibrations. During the 2014-037/038 pass, TPR filters were used that were too wide such that LRO's 2.3-GHz signal corrupted the noise temperature measurements when LRO was in front of the Moon. These problems were resolved for the remaining passes starting on 2014-045 as appropriate filters were used and calibrations performed (see Table 2, page 15). Thus, the noise temperature data collected from 10 tracking passes (see Table 2, page 15) were used in changing data rate link scenario calculations to determine link advantage over different orbit projections, frequency bands, and lunar phase angles.

Pointing at the lunar center, limbs, and cold sky (±3 deg offsets in cross-elevation) was achieved using the station's planetary predict mode. It was found that there was a sizable pointing error for several of the passes, but it was established that the effect on the error in differencing measurements while pointed at disk center and at the cold sky (3 deg points) was negligible and thus did not significantly alter the lunar noise temperature increase results. The limb-centered measurements showed significant asymmetry as they were more sensitive to the pointing error and thus were not used in this analysis. The predictions used to point the antenna at the LRO spacecraft using the station's AZ–EL predict mode were correct and thus there was negligible pointing error. Thus, it was established that the issue with planetary mode pointing was not a problem for the purpose of this study. This was supported by the facts that (1) the calibrations produced results that were in general agreement with previous measurements [1], and (2) that the noise temperature peaks while tracking LRO at or close to the point of disk center were comparable to those of the lunar disk center measurements in planetary mode.

III. Lunar Orbit Types and Resulting Signatures

Pass 2014-045 is an example of an intermediate orbit-crossing signature where the position of LRO in its orbit midway across the lunar disk falls between the center and the limb, as shown in Figures 1 and 2. Pass 2014-047 is an example of a disk center crossing orbit where the mid-point of LRO's orbit across the disk of the Moon falls very close to the disk center. Figure 5 displays the 2.3-GHz system noise temperature sequence for this case and Figure 6 displays the 8.4-GHz signature in system noise temperature. Figure 7 displays a SOAP image of the lunar disk for 2014-047 along with the orbit of LRO.

Pass 2014-055 is an example of a "limb-hugging" orbit where the LRO orbit encircles the lunar disk in a nearly "face-on" orientation in the plane of the sky. Figure 8 displays the 2.3-GHz system noise temperature sequence for this case and Figure 9 displays the corresponding 8.4-GHz system noise temperature signature. Figure 10 displays a SOAP image of the lunar disk along with the "limb-hugging" orbit of LRO for this pass. The annotated points A through G in Figures 8 and 9 can be correlated with the locations of LRO in its orbit shown in Figure 10.

The measured noise temperature signatures as LRO orbits the Moon appear to be "sinusoidal-like" and smooth. That is, there are no significant short time-scale "wiggles" such as

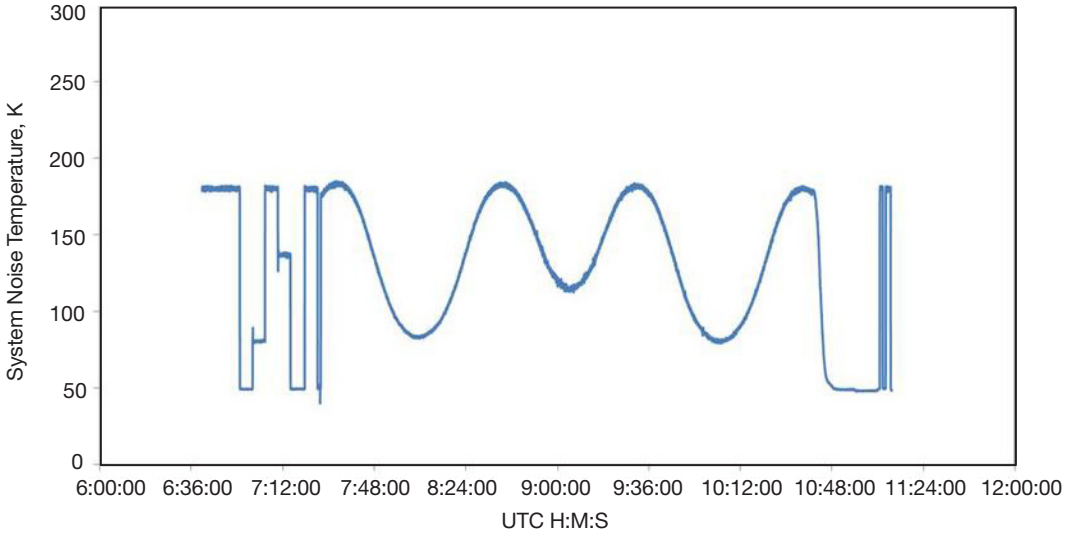

Figure 5. 2.3-GHz noise temperature measurements during DSS-13 tracking pass 2014-047.

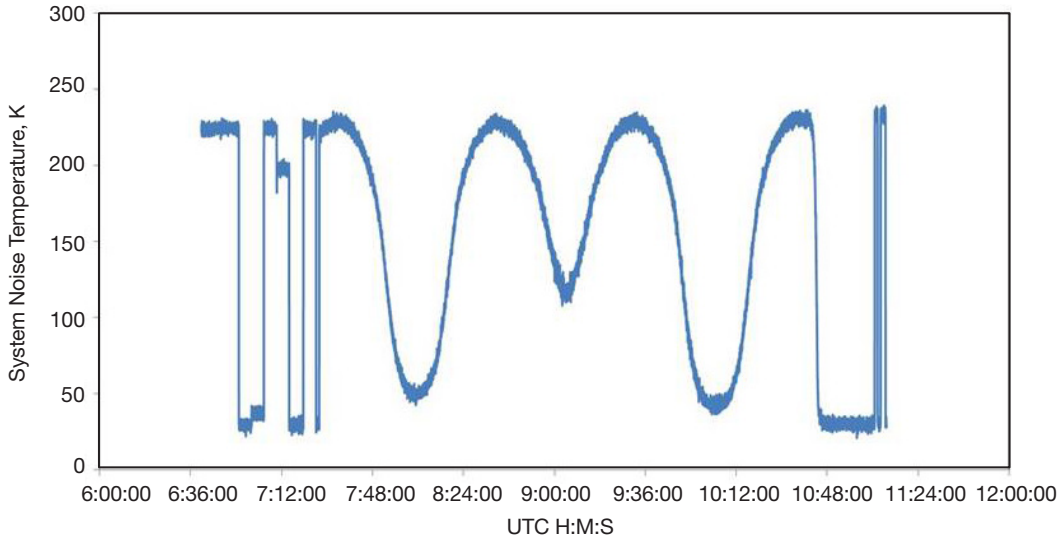

Figure 6. 8.4-GHz noise temperature measurements during DSS-13 tracking pass 2014-047.

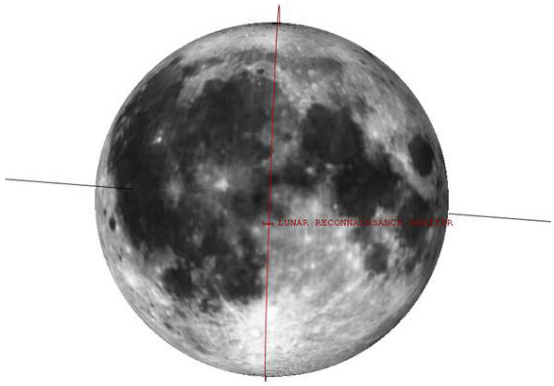

Figure 7. SOAP image of Moon on 2014-047 showing LRO in a disk center crossing orbit. Lunar phase angle = 183.5 deg (near-full moon).

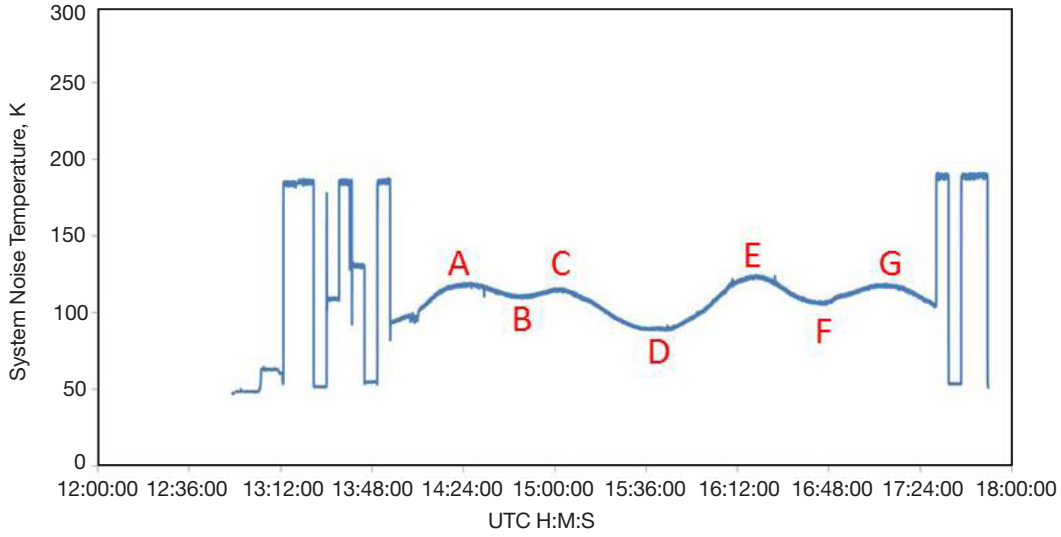

Figure 8. 2.3-GHz noise temperature measurements during DSS-13 tracking pass 2014-055.

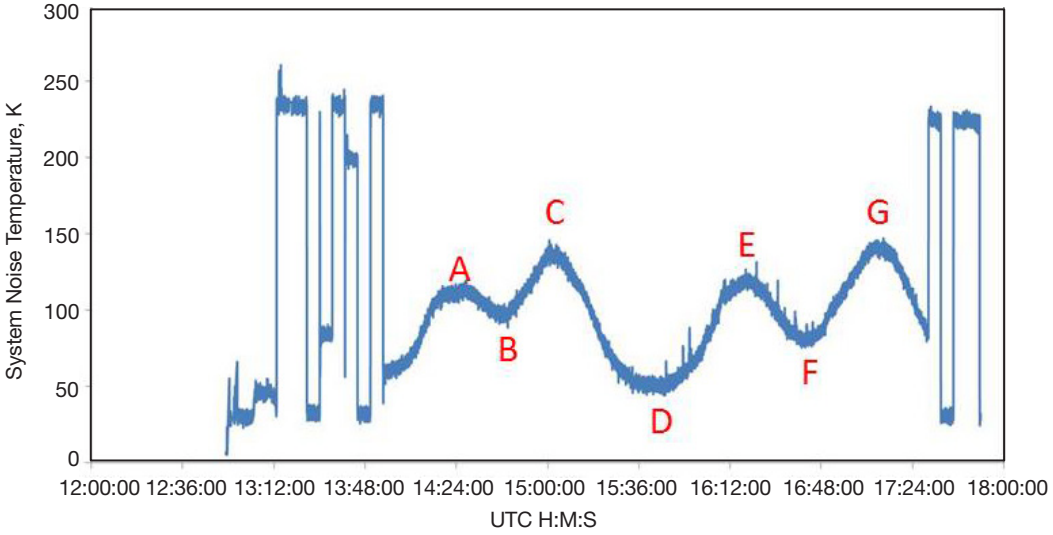

Figure 9. 8.4-GHz noise temperature measurements during DSS-13 tracking pass 2014-055.

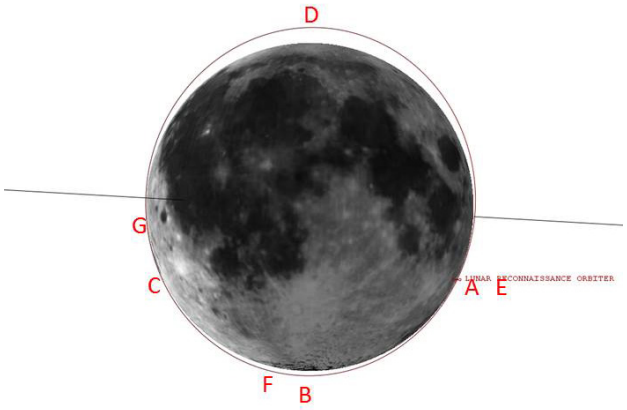

Figure 10. SOAP image of Moon on 2014-055 showing LRO in a "limb-hugging" face-on orbit orientation about the lunar disk. Lunar phase angle = 326 deg (thin crescent).

would be expected due to significant differences in noise temperature with differing terrain (lighter regions cooler and darker regions hotter). This implies that the convolution of the antenna beam against the lunar disk tends to smooth out any such small-scale differences due to terrain and lunar phase differences.

The peaks in the LRO noise temperature signatures appear to be at or below the disk-centered lunar noise temperature measurements performed near the beginning and end of the pass, as expected. The troughs in the noise temperature signature appear consistent with where LRO is in its orbit — higher values when LRO is at a limb at largest excursion with low altitude and lower values when LRO is near a limb at largest excursion with high altitude. The noise temperature increase measured for LRO at its highest altitude away from the limb at cold sky is evidently a larger effect than due to lunar phase (whether the limb is illuminated or not).

IV. Dynamic Link Advantage Tracking a Lunar Orbiter

When tracking a lunar orbiter, the amount of data that can be returned depends upon the signal-to-noise ratio (SNR) of the received signal. When the orbiter is near a limb of the Moon, the ground antenna beam receiving the signal picks up less of the lunar disk and more of the cold sky. Thus, a lower noise temperature allows for a higher SNR and thus a higher data rate. When the orbiter is crossing near the center of the lunar disk, the noise temperature is near maximum and thus the SNR is near its lowest value and the orbiter must be operating at a lower data rate. Given that the lunar noise temperature increase is substantial relative to the nominal operating noise temperature, a large increase in data volume can be realized by judiciously stepping or changing the data rate as the SNR changes during the course of a lunar orbit. Most telecommunications link budgets usually assume a single-point configuration based on worst-case conditions. Such link scenarios may assume maximum range distance, minimum elevation angle, and (for lunar tracking) a "worst-case" lunar noise temperature contribution expected when pointed at the lunar disk center. Such link budgets thus accommodate the lowest possible data rate. The data volume return during a lunar orbit can be increased by dynamically changing the data rate in step with the SNR as a function of orbiter position across the lunar disk (as the ground antenna beam picks up different contributions of cold sky and lunar disk). In addition, due to the nature of dynamics in the orbit, more data can be returned at higher data rates near the lunar limbs (since the orbiter spends more time here) versus against the disk center (as the orbiter angular speed relative to Earth is higher).

For the purpose of this article, we take the raw DSS-13 system noise temperature measurements of LRO in its orbit, and refer them to that of an operational DSN station at either 2.3 GHz or 8.4 GHz. This involves taking each LRO system noise temperature at DSS-13, T_{sys_13}, and subtracting out the background cold-sky system noise temperature T_{off} for the track (~30 K to 50 K). To refer the system noise temperature to that of a higher-performance system such as an operational DSN station, we add 25 K back in. Thus, an operational DSN background noise temperature (25 K) is added back in to refer the system noise temperature to that of the higher-performance system. It should be pointed out that the actual background noise temperature to be added back in will depend upon the individual DSN station, its elevation angle, and its microwave configuration (whether the diplexer is in

or out). The reader is thus referred to [5] to make use of any differences from this simple assumption used here. For many scenarios, the background DSN antenna and equipment temperature will lie close to 25 K for an operational DSN station, and this provides a reasonable background level in which to access link advantage. Thus,

$$T_{sys\_new} = T_{sys\_13} - T_{off} + 25 \quad (K). \tag{1}$$

The dB difference or advantage A relative to the disk-centered noise temperature is then estimated as follows:

$$A = 10 \log_{10}\left[T_{sys\_new}/\left(T_{Moon} + 25\right)\right]. \tag{2}$$

Here, T_{Moon} is the "worst-case" disk-centered lunar noise temperature obtained from the differences of the disk-centered and ±3 deg cold-sky measurements. This dB difference in Equation (2) varies with the position of a lunar orbiter in its orbit, taking on higher values near the limbs and lower values near the disk center. The signatures are different for 2.3 GHz and 8.4 GHz, as can be seen in Figures 11 and 12 for 2014-047, Figures 13 and 14 for 2014-055, and Figures 15 and 16 for 2014-045, respectively, for the different orbit projections against the lunar disk.

For the purpose of determining the advantage by changing the data rate as the SNR varies due to the changing noise temperature, we first assume a worst-case scenario where we establish a reference data volume. This assumes a static data rate over the entire orbit based on sizing the link using the noise temperature when pointed at the disk center. We assume a constant data rate R in bps. We then take each data point over each 1-s interval that LRO is tracked such as shown in Figures 11 and 12 for 2014-047. The achieved data volume using the static worst-case data rate is then calculated as $V_{ref} = R\Delta T$, where ΔT (in seconds) is the entire period that LRO is being tracked. For now, we include the periods when LRO is behind the Moon and assume the resulting noise temperature signature and hence link advantage is valid.

Next, we address the case where we change the data rate to R_i for the ith 1-s interval by multiplying the baseline data rate R by the link advantage for that 1-s point:

$$R_i = R10^{A_i/10}$$

where A_i is the advantage for the ith data point [Equation (2)]. We then multiply this data rate by the time difference for each individual data interval $\Delta T_i = t_i - t_{i-1}$ and sum up over all of the data points from $i = 2$ to N to get the achieved data volume V:

$$V = \sum_i R_i \Delta T_i.$$

The achieved data volume V is then compared to the baseline (static data rate) data volume V_{ref} to infer the amount of data one could return with such a scheme, V/V_{ref}, as shown in Table 2 (color-coded "S-band Volume Gain" and "X-band Volume Gain" columns).

Table 2 summarizes the estimated link advantage results for each of the LRO tracking passes at both 2.3 GHz and 8.4 GHz. The lunar phase angle and mean elevation angle for each

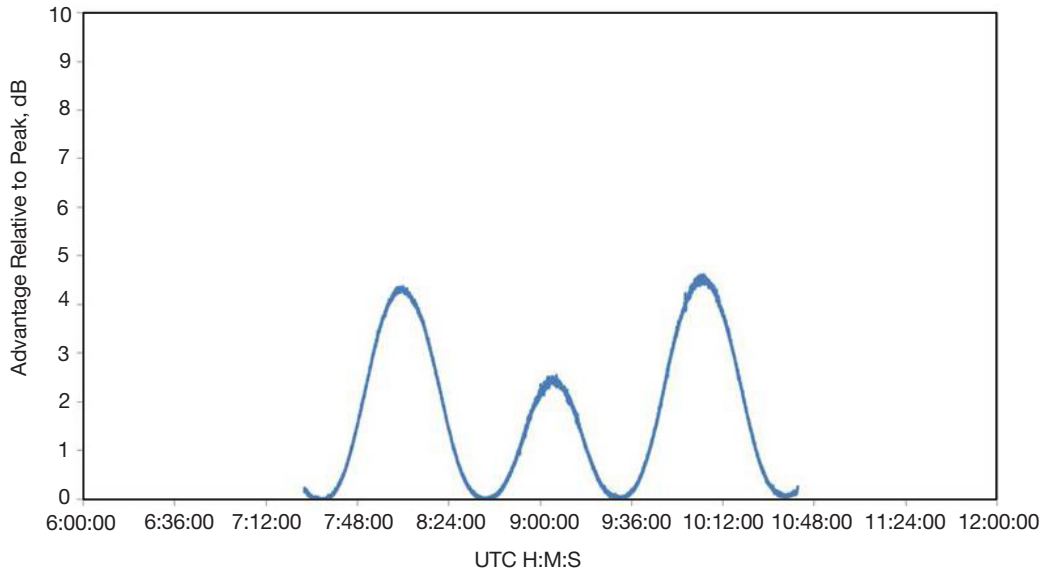

Figure 11. Estimated link advantage as a function of time extracted from noise temperature measurements for disk center crossing pass 2014-047 at 2.3 GHz.

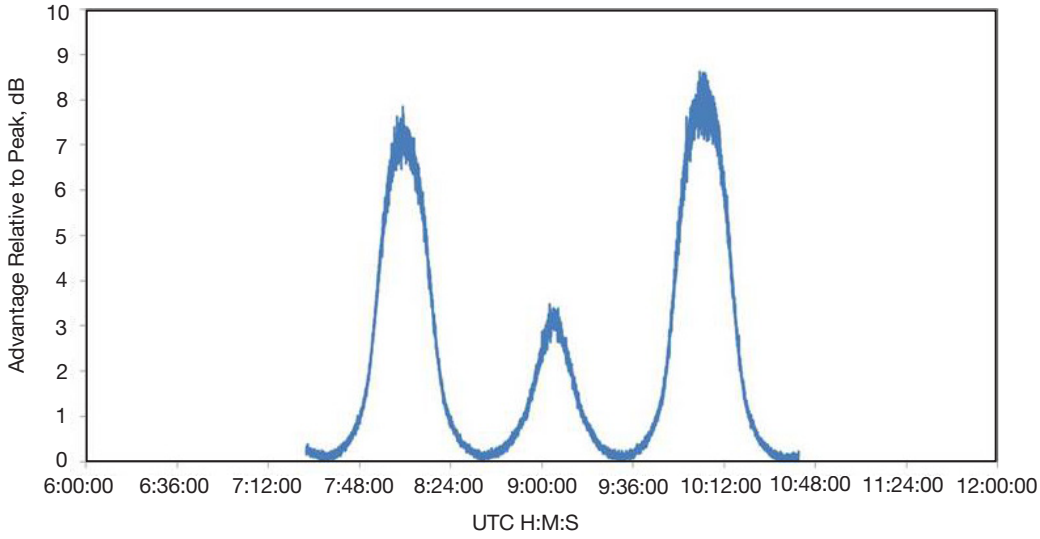

Figure 12. Estimated link advantage as a function of time extracted from noise temperature measurements for disk center crossing pass 2014-047 at 8.4 GHz.

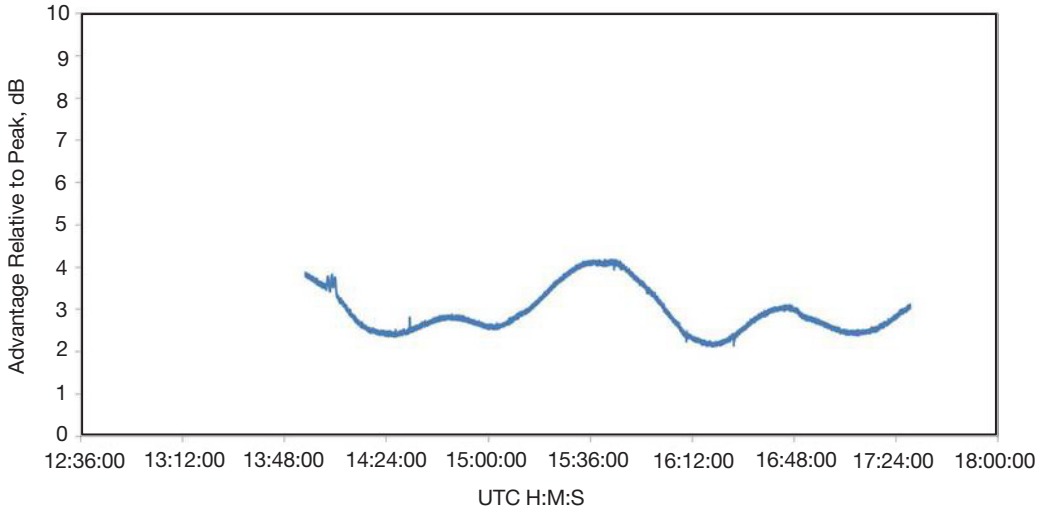

Figure 13. Estimated link advantage as a function of time extracted from noise temperature measurements for "limb-hugging" orbit pass 2014-055 at 2.3 GHz.

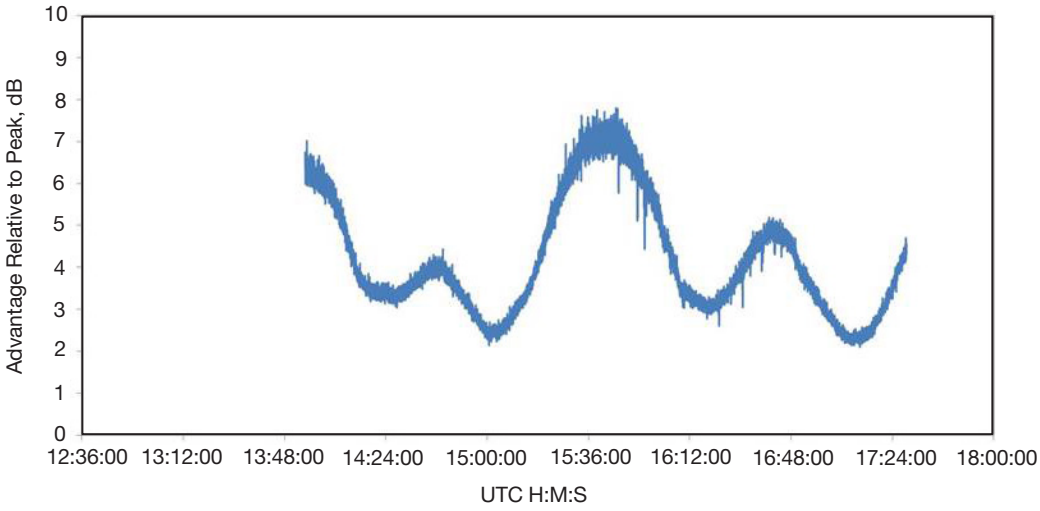

Figure 14. Estimated link advantage as a function of time extracted from noise temperature measurements for "limb-hugging" orbit pass 2014-055 at 8.4 GHz.

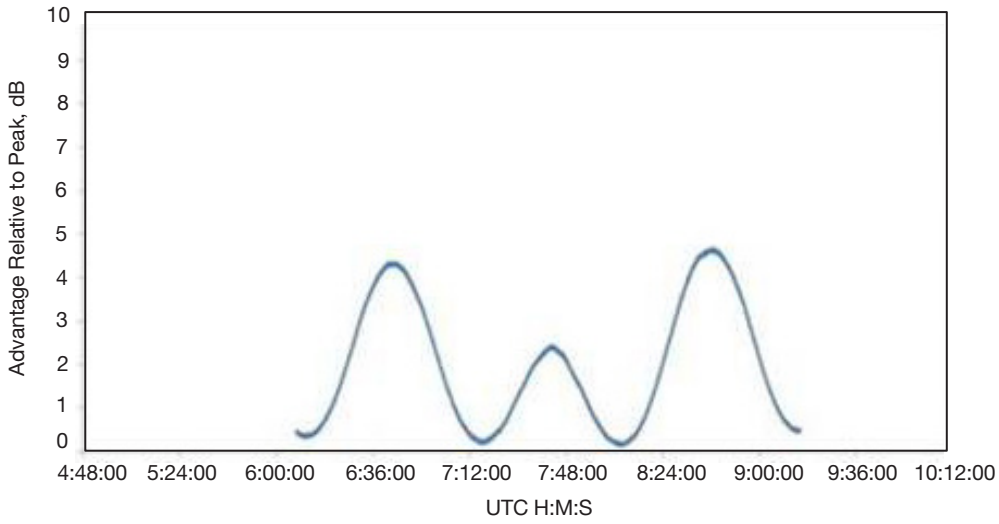

Figure 15. Estimated link advantage as a function of time extracted from noise temperature measurements for intermediate disk crossing orbit pass 2014-045 at 2.3 GHz.

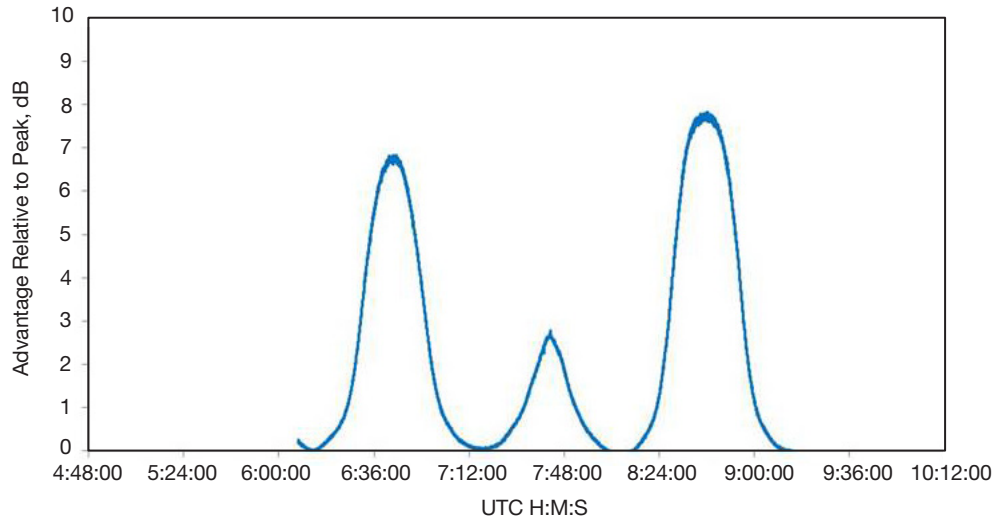

Figure 16. Estimated link advantage as a function of time extracted from noise temperature measurements for intermediate disk crossing orbit pass 2014-045 at 8.4 GHz.

Table 2. Achieved data volume (assuming "continuous" data rate adjustment).

Pass	Day of Year	Days Past Jan 1, 2013	Lunar Phase Angle, deg	Mean Elevation, deg	Data Volume, bits	S-band Volume, bits	S-band Volume Gain	X-band Volume, bits	X-band Volume Gain	S-band Max, dB	S-band Min, dB	X-band Max, dB	X-band Min, dB	Altitude at Max, km	Orbit Projection Type
2014-045	45	410	178.9	54.4	112.62	188.44	1.67	229.47	2.04	4.69	0.13	7.83	–0.18	180.21	I
2014-047	47	412	183.5	49.5	116.69	183.88	1.58	233.92	2.00	4.62	–0.07	8.62	–0.03	173.47	C
2014-049	49	414	199.9	41.3	115.37	186.83	1.62	217.84	1.89	4.35	0.09	7.56	–0.33	90.41	I
2014-051	51	416	228.9	34.8	118.93	225.96	1.90	286.67	2.41	4.47	1.28	7.40	0.53	173.26	I/LH
2014-055	55	420	326.5	28.37	127.37	252.98	1.99	356.40	2.80	4.19	2.13	7.80	2.10	168.08	LH
2014-058	58	423	353.2	36.3	114.61	172.89	1.51	193.76	1.69	4.39	0.06	7.61	–0.25	169.89	I
2014-065	65	430	63.3	59.4	120.85	240.35	1.99	423.28	3.50	4.60	1.59	9.96	0.25	159.77	LH
2014-070	70	435	133.0	70	122.80	239.30	1.95	371.97	3.03	4.46	1.00	8.85	–0.29	185.58	I/LH
2014-073	73	438	169.5	63	122.83	191.87	1.56	236.62	1.93	4.63	–0.08	9.19	–0.32	177.00	C
2014-076	76	441	180.9	42.3	122.88	199.98	1.63	269.01	2.19	4.94	–0.14	9.02	–0.06	167.70	I
I or C		I/LH or LH													

I = Intermediate; C = Center-crossing; LH = Limb-hugging

pass is tabulated along with the nominal data volume, assuming a worst-case link budget for the pass (uses single-point lunar noise temperature as measured at the center of the lunar disk). Also tabulated are the achievable data volumes for 2.3 GHz and 8.4 GHz by making use of the DSS-13 measured noise temperatures over each LRO pass and adjusting them accordingly using Equation (1) to reference them to that of an operational 34-m-diameter DSN station.

We included the portion of the orbit where LRO is behind the Moon. Since we can observe a near-symmetry in the signature when LRO is in front of and behind the Moon (see, for example, Figures 1 and 2), we can assume the reference data volume and achieved data volume just scale by 1/2, leaving essentially the same data volume advantage. This would be applicable for both 2014-045 and 2014-047 orbit projection types. For the case of the limb-hugging orbit, such as for 2014-055, we see that LRO is essentially visible during the entire orbit, and the data volume advantage achieved is again valid.

In practice, we will not continuously step the data rate every second, but instead make use of an operationally simpler scenario such as employing three different data rate periods during an orbit. A lower data rate would be utilized when the spacecraft is crossing near disk center, where the noise temperature is higher. A higher data rate would be utilized when the spacecraft is transiting near the limbs where the noise temperature is lower. Further discussion of such data rate stepping can be found in [6].

The maximum and minimum dB link advantages in data rate over each pass are also shown in Table 2. The second to last column of Table 2 shows the altitude of the LRO orbiter above the lunar surface at the time of maximum data rate advantage when the beam pickup of cold sky is at its maximum, and pickup of lunar disk temperature is at its minimum over the pass. The last column depicts the orbit type: C for center-crossing, I for intermediate, and LH for limb-hugging. The designation I/LH is used to designate that most of each side of the LRO orbit crosses the disk close to each lunar limb.

For orbits that cross at or near the lunar center, we make use of the results from several disk-center crossing passes, such as 2014-045 and 2014-047 (see Figures 11 and 12, and Figures 15

and 16). The 2.3-GHz dB advantage relative to disk center ranges from 4.51 dB to 0.05 dB and can return a factor of 1.59 ±0.07 more data (average and standard deviation of yellow highlighted cells in Table 2). The 8.4-GHz dB advantage relative to disk center ranges from 7.99 dB to close to 0 dB (–0.25 dB) and returns a factor of 1.90 ±0.15 more data (average and standard deviation of yellow highlighted cells in Table 2). These factors assume that the data rate can be continuously changed. In practice, the data return will be lower as one will likely change data rate in discrete steps instead of continuously [6]. These estimates are based on an LRO orbit where the highest altitude above the surface at the limb varies from 90 km to 180 km. The results for other orbiting spacecraft will differ depending upon orbit shape, and minimum and maximum altitude above limbs.

For orbits that are limb-hugging, we make use of the results from the orange highlighted passes (see Table 2), such as the example of pass 2014-055 showing the 2.3-GHz advantage in Figure 13 and the 8.4-GHz advantage in Figure 14. The 2.3-GHz dB advantage relative to disk center ranges from 4.43 dB to 1.50 dB and can return a factor of 1.96 ±0.04 more data. The 8.4-GHz dB advantage relative to disk center ranges from 8.67 dB to 0.48 dB and returns a factor of 2.98 ±0.48 more data. These factors assume that the data rate can be continuously changed. In practice, the achievable data return will be lower as one will likely change data rate in few discrete steps instead of continuously [6].

For orbits that are intermediate, we make use of the result from pass 2014-045 showing the 2.3-GHz advantage in Figure 15 and the 8.4-GHz advantage in Figure 16. The results lie somewhere in between those of limb-hugging and disk center crossing orbits.

The effect of any systematic calibration errors, such as at the 4 percent level, results in a much smaller error in the noise temperature differences, and hence the link advantage (less than 0.1 dB). This translates to less than ~1 percent error in achievable data volume advantage.

V. Conclusion

We have quantified the increase in data return that can be realized by tracking a lunar orbiter using a 34-m-diameter antenna at 2.3 GHz and 8.4 GHz, using LRO lunar noise temperature measurements. The 2.3-GHz advantage can be as high as 4.4 dB and for 8.4 GHz as high as 8.6 dB, assuming a continuously variable data rate. The actual advantage will lie somewhat below that depending upon data rate stepping, where higher data rates will be used near the lunar limbs where there is more cold sky pickup and high duration of orbiter visibility relative to tracking near the disk center. The advantage realized by continuously changing the data rate to accommodate changing SNR relative to using a static worst-case data rate was shown to be a factor of two times more data at 2.3 GHz and a factor of three times more data at 8.4 GHz. In practice, the data return will be lower due to utilizing fewer data rate changes during an orbit for operational considerations. Additional work being considered includes examining different orbit types such as more inclined orbits (high elliptical orbits) at each of the frequencies. A future study being considered is examining the link advantage that is achievable during a lunar orbit at the near-Earth Ka-band frequency allocation at 26 GHz.

Acknowledgments

I would like to thank Kar-Ming Cheung for supporting this study, the DSS-13 operations staff for conducting the experiments, Larry Teitelbaum and Watt Veruttipong for providing station configuration information, and Chuck Naudet for providing review comments. I would also like to also thank Kenneth Chan for assistance with DSS-13 pointing issues. I would like to thank Behzad Raofi and the LRO Project (especially Ralph Casasanta of NASA's Goddard Space Flight Center) for their assistance and cooperation.

References

[1] D. D. Morabito, W. A. Imbriale, and S. Keihm, "Observing the Moon at Microwave Frequencies Using a Large-Diameter Deep Space Network Antenna," *IEEE Transactions on Antennas and Propagation*, vol. 56, no. 3, pp. 650-660, March 2008. http://ieeexplore.ieee.org/xpl/articleDetails.jsp?arnumber=4463904

[2] C. Stelzried and M. Klein, "Precision DSN Radiometer Systems: Impact on Microwave Calibrations," *Proceedings of the IEEE*, vol. 82, no. 5, pp. 776–787, May 1994. http://ieeexplore.ieee.org/xpl/articleDetails.jsp?arnumber=284745

[3] NASA Goddard Space Flight Center, "Radio Frequency Interface Control Document (RFICD) Between Lunar Reconnaissance Orbiter (LRO) and the Near Earth Network (NEN), Deep Space Network (DSN), and Space Network (SN)," 450-RFICD-LRO/NEN/DSN/SN, Revision 1, February 2009.

[4] D. Y. Stodden and G. D. Galasso, "Space System Visualization and Analysis Using the Satellite Orbit Analysis Program (SOAP)," *Proceedings of the 1995 IEEE Aerospace Applications Conference*, Aspen, Colorado, February 4–11, 1995. http://ieeexplore.ieee.org/stamp/stamp.jsp?arnumber=00468892

[5] S. D. Slobin, "34-m BWG Stations Telecommunications Interfaces," *DSN Telecommunications Link Design Handbook*, DSN No. 810-005, Module 104, Rev. G, Jet Propulsion Laboratory, Pasadena, California, March 5, 2013. http://deepspace.jpl.nasa.gov/dsndocs/810-005/104/104G.pdf

[6] K.-M. Cheung, C.-W. Lau, and C. Lee, "Link Analysis for Space Communication Links Using ARQ Protocol," *Proceedings of IEEE Aerospace Conference*, pp. 1–8, Big Sky, Montana, March 1–4. http://ieeexplore.ieee.org/xpls/abs_all.jsp?arnumber=6836210